JACS
JOURNAL OF THE AMERICAN CHEMICAL SOCIETY
pubs.acs.org/JACS
Article

Luminescent Quantum Dots Stabilized by N-Heterocyclic Carbene Polymer Ligands

Liang Du, Neda Arabzadeh Nosratabad, Zhicheng Jin, Chengqi Zhang, Sisi Wang, Banghao Chen, and Hedi Mattoussi*

Cite This: J. Am. Chem. Soc. 2021, 143, 1873−1884
Read Online
ACCESS | Metrics & More | Article Recommendations | Supporting Information

ABSTRACT: We have tested the ability of N-heterocyclic carbene (NHC)-modified ligands to coordinate and stabilize luminescent CdSe−ZnS core−shell quantum dot (QD) dispersions in hydrophilic media. In particular, we probed the effects of ligand structure and coordination number on the coating affinity to the nanocrystals. We find that such NHC-based ligands rapidly coordinate onto the QDs (requiring ∼5−10 min of reaction time), which reflects the soft Lewis base nature of the NHC groups, with its two electrons sharing capacity. Removal of the hydrophobic cap and promotion of carbene-driven coordination on the nanocrystals have been verified by ^{1}H NMR spectroscopy, while ^{13}C NMR was used to identify the formation of carbene−Zn complexes. The newly coated QD dispersions exhibit great long-term colloidal stability over a wide range of conditions. Additionally, we find that coordination onto the QD surfaces affects the optical and spectroscopic properties of the nanocrystals. These include a size-dependent red-shift of the absorption and fluorescence spectra and a pronounced increase in the measured fluorescence intensity when the samples are stored under white light exposure compared to those stored in the dark.

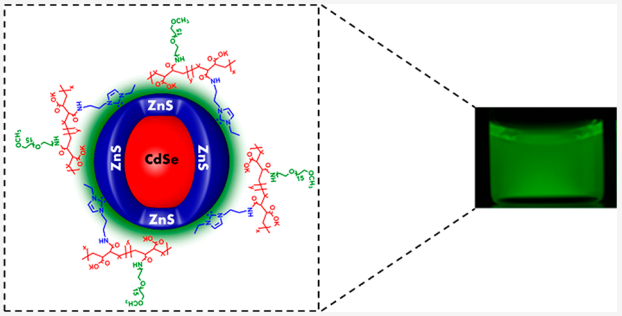

INTRODUCTION

N-heterocyclic carbenes (NHCs) have been widely investigated since their synthesis and isolation by Arduengo and co-workers in 1991.[1,2] Because of their reported strong coordination to transition metals, NHC compounds have been tested in a variety of catalytic applications such as cross-coupling and olefin metathesis.[3−7] Positioned between two adjacent π-donating nitrogen atoms, the carbene lone pair exhibits outstanding stability under inert conditions. Once the lone-pair electrons donated into the σ-accepting orbital of a transition metal, the NHC−metal complexes can be air stable for weeks either in solution or as a solid.[8] Because of the unique electronic stability of these structures, complexes of NHCs have been used to target and interact with biomolecules in physiological conditions.[9] For example, gold−NHC complexes have been developed as anticancer agents, and their reactivity with ubiquitous thiol-containing biomolecules has been widely investigated.[10−12] Platinum− and palladium−NHC complexes display biological stability, and it has been reported that Pt(II)−NHC and Pd(II)−NHC based antitumor drugs exhibit great potency against human cancer cells.[13−16] In recent years, NHC-containing compounds have been utilized to passivate metallic nanomaterials in both organic and aqueous media. For instance, a bidentate NHC−thioether ligand has been reported to stabilize palladium nanoparticles in both protic and aprotic solvents, and the resulting hybrid shows great chemoselectivity for hydrogenation of olefins.[17] Ruthenium nanoparticles stabilized by NHC-containing ligands act as nanocatalysts for arene hydrogenation, as reported by van Leeuwen and co-workers.[18] Detailed studies by the groups of Johnson and Crudden have demonstrated that gold nanoparticles and nanorods coated with NHC-modified ligands can be stable under various conditions.[19,20] Glorius and co-workers reported on the ability of alkyl-appended NHC molecules to stabilize upconverting nanoparticles made of Tm-doped $NaYF_4$:Yb cores.[21] They further showed that the resulting NPs were capable of inducing trans-to-cis isomerization of azobenzene molecules. More recently, He and co-workers have prepared a few NHC-terminated polymers and reported that they can stabilize gold nanoparticle dispersions in either organic or aqueous conditions for a few months.[22] However, these studies have mainly focused on nanocolloids made of the noble metal cores, while fewer studies have investigated the use of NHC compounds to stabilize other nanocrystals, namely fluorescent materials.[21]

Received: October 5, 2020
Published: January 15, 2021

https://dx.doi.org/10.1021/jacs.0c10592
J. Am. Chem. Soc. 2021, 143, 1873−1884

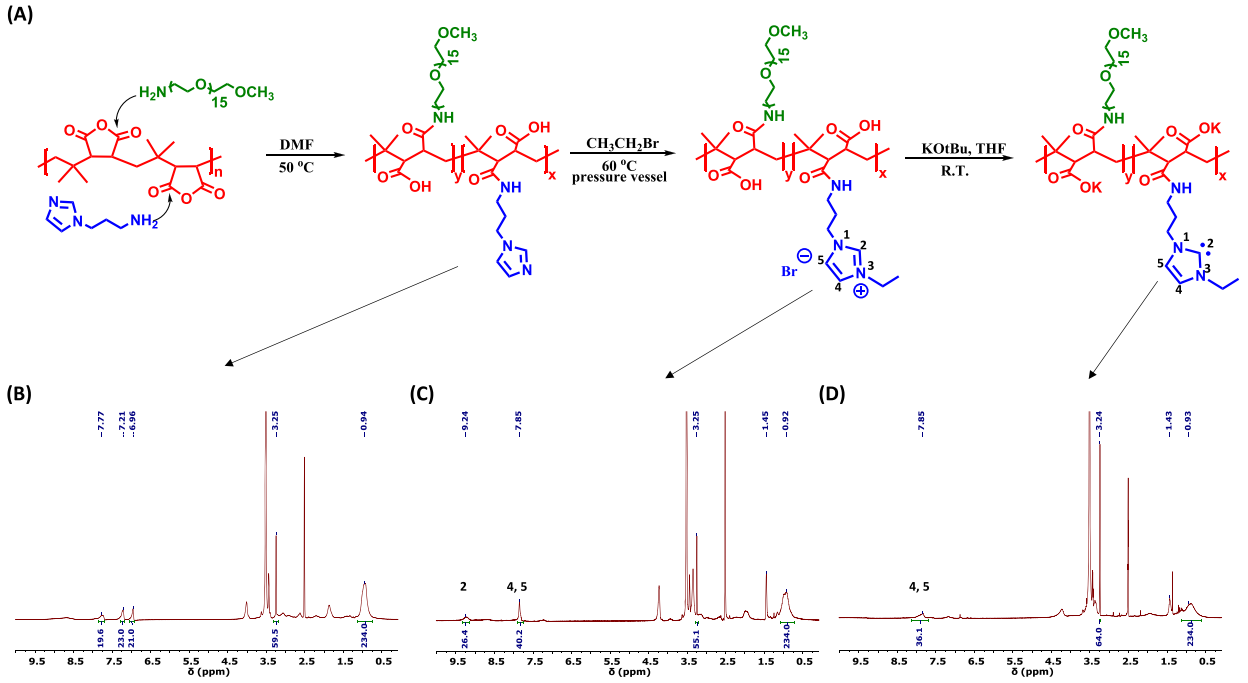

Figure 1. (A) Schematic representation of the nucleophilic addition reaction used to prepare the multicoordinating polymer ligands. (B) ^{1}H NMR spectrum of APIm-PIMA-PEG in DMSO-d_6. The peaks at 3.5 and 3.25 ppm emanate from the PEG block and terminal methoxy protons, respectively. The stoichiometry was estimated by comparing the integration values of the peaks attributed to $-\mathbf{OCH_3}$ (3 H, 3.25 ppm) and imidazole (3 H on the heterocyclic ring, ∼6.96, 7.21, and 7.77 ppm) with the peak ascribed to the methyl groups in the PIMA backbone (∼234 H, ∼0.9 ppm). (C, D) ^{1}H NMR spectra of APEIm-ium-PIMA-PEG and NHC-PIMA-PEG collected in DMSO-d_6. The carbene generation is confirmed by the absence of the peak at 9.24 ppm, which is ascribed to the proton on C2 in the heterocyclic ring. The signature at ∼2.5 ppm is from DMSO.

NHC-supported zinc species exhibit low toxicity, electronic tunability, and steric stability, which have motivated their use in reduction catalysis.[23] This suggests that NHC-appended molecules would be great for surface-stabilizing zinc-rich nanocrystals. Semiconductor nanocrystals (quantum dots, QDs) overcoated with ZnS shells have been greatly investigated over the past two decades, given their unique photophysical properties.[24−27] They have also been integrated into a variety of applications, including optoelectronic devices and as fluorescent probes in biology.[28−33] Stabilization of these materials has exploited an array of bifunctional molecules which bind onto the QD surface via Lewis acid and/or Lewis base interactions. There has been an ever-growing interest in exploring additional ligands that present high affinity stable coordinating groups. For example, several strategies have been developed for preparing biocompatible QDs, relying on cap exchange with coordinating ligands.[34,35] This strategy is attractive as it yields NPs with a compact coating and tunable functionalities.[36−38] Thiol-based ligands are one of the most utilized candidates to stabilize an array of nanocrystals in aqueous solutions.[26,39−45] Alternatively, imidazole has been shown to coordinate onto different types of nanocolloids, and it is beneficial to QD fluorescence.[46−51] Hydrophilic phosphonate-modified ligands have also been shown to impart great colloidal stability onto distinct inorganic nanocrystals, including semiconductor, metallic, and magnetic cores in water media.[52−56] Cap exchange with these ligands often requires long reaction time (hours to overnight), which sometimes complicates the phase transfer steps. Therefore, developing alternative anchoring molecules that can promote rapid ligand substitution, while yielding nanocrystals with good biostability, is highly desired and actively sought.

In this report, we demonstrate the ability of NHC-modified polymer to promote rapid ligand substitution on luminescent QDs. In particular, we find that a low molecular weight polymer combining several NHC groups and poly(ethylene glycol) (PEG) blocks can promote the dispersion of several color QDs in buffer media while preserving their optical properties. This ligand design takes advantage of the highly efficient nucleophilic addition reaction between amine-R nucleophiles and a low molecular weight poly(isobutylene-*alt*-maleic anhydride), PIMA.[51,57−59] NHC groups were generated by quaternization and deprotonation of the imidazole rings. A complete substitution of the native coating requires only 5−10 min of mixing, as has been confirmed by 1- and 2-D ^{1}H, ^{13}C NMR spectroscopy. Cap exchange using NHC-polymer yields QDs that are dispersible in buffer media over a broad range of biological conditions. Additionally, the coating yields QDs with compact sizes as confirmed by diffusion ordered NMR spectroscopy (DOSY).

RESULTS AND DISCUSSION

Ligand Design. Given the excitement generated in the community to understand the nature of NHC coordination onto a variety of transition metal atoms or surfaces, designing various NHC containing structures and testing their binding affinity onto colloidal inorganic nanocrystals will provide valuable information about those interactions. It can further expand the utility of such groups in materials chemistry and nanotechnology. Additionally, it has been widely accepted that coordination of various ligands onto transition metal atoms, ions, and surfaces would usually benefit from multidentate interactions.[60−63] Thus, installing several NHC groups along

https://dx.doi.org/10.1021/jacs.0c10592
J. Am. Chem. Soc. 2021, 143, 1873−1884

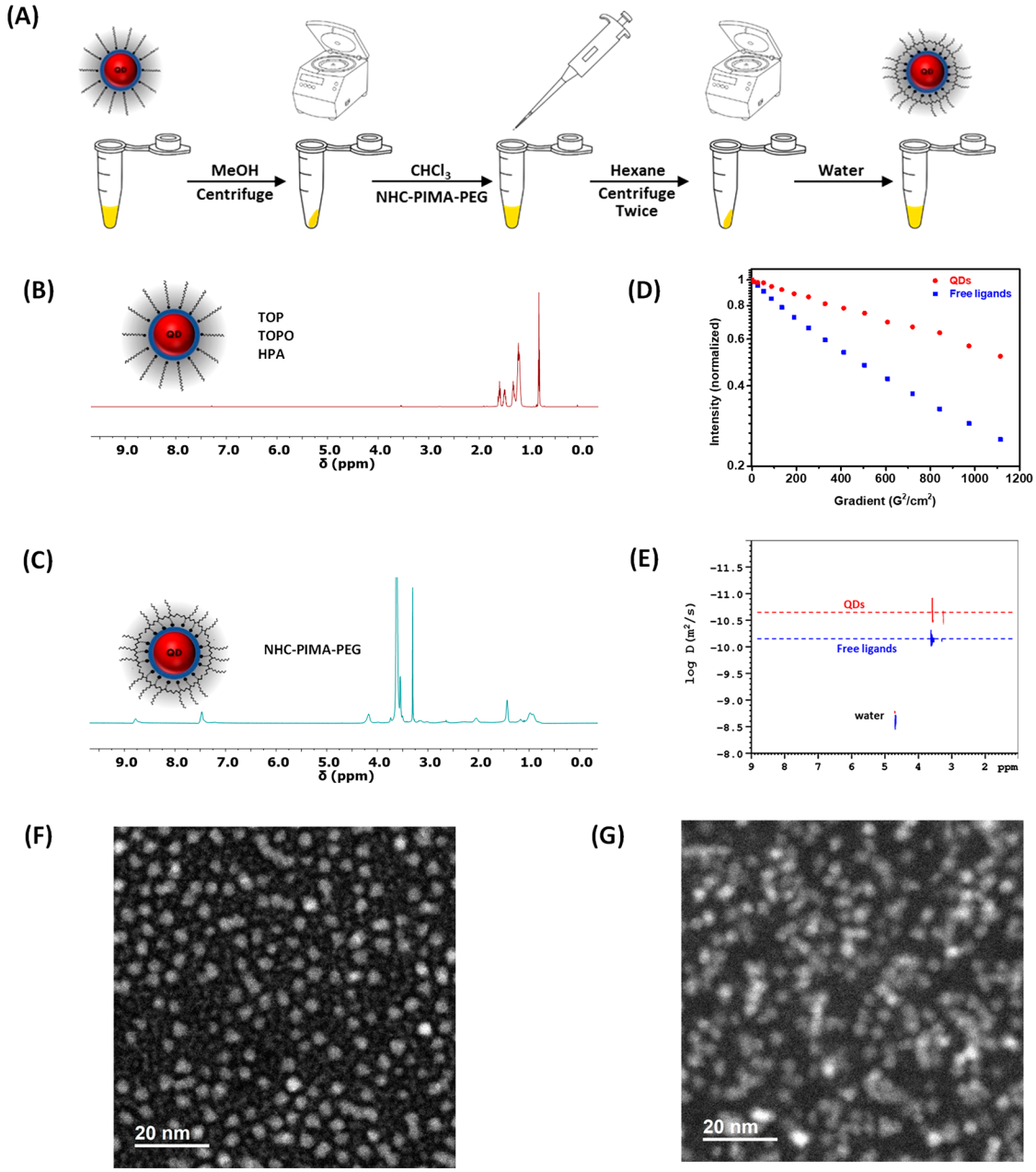

Figure 2. (A) Schematic depiction of the ligand exchange (icons from www.labicons.net) using NHC-PIMA-PEG. (B, C) ^{1}H NMR spectra of QD dispersions before and after ligand exchange, collected in $CDCl_3$ and D_2O, respectively. Water suppression was applied to the spectrum collected from the aqueous sample. (D, E) Plots of the normalized NMR signal intensity vs G_z^2 collected from QD and free ligand samples along with the corresponding two-dimensional DOSY contour spectra measured in D_2O. (F, G) HAADF-STEM images acquired from the as-grown QDs capped with the native ligands (left, average diameter ~3.3 nm) and NHC-polymer-capped QDs (right, average diameter ~3.2 nm). We should note that the blurriness in the image acquired from the polymer-QD sample (shown in part G) is due to the polymeric coating on the nanocrystals which broadens the image-forming probe, resulting in lower resolution.

the backbone of a low molecular weight polymer, where control over the structure and stoichiometry can be achieved, would provide a great NHC-based ligand to test. To attain this goal, we have exploited some of the unique features of the one-step nucleophilic addition reaction between amine-R nucleophiles and the poly(isobutylene-*alt*-maleic anhydride) copolymer to attach several NHC groups along a PIMA chain.[37,49,58,59,63] This yields a multi-NHC ligand that exhibits rapid and robust coordinating interactions with ZnS-overcoated CdSe quantum dots. This synthesis route allows easy tuning of the ligand stoichiometry by adjusting the molar fraction of the various precursors. Figure 1A schematically summarizes the reaction steps starting with 1-(3-aminopropyl)imidazole (APIm), PIMA, and NH_2-PEG-OCH_3; the precursor NH_2-PEG-OCH_3 is prepared via amine modification of OH-PEG-OCH_3 following previous protocols reported by our group, while commercially available APIm is used.[64] The reaction mixture is heated in DMF, and the product APIm-PIMA-PEG can be directly quaternized by bromoethane to yield an imidazolium-presenting intermediate, APEIm-ium-PIMA-PEG. The volatile bromoethane can be easily removed, and the pure product can be collected with a

https://dx.doi.org/10.1021/jacs.0c10592
J. Am. Chem. Soc. 2021, 143, 1873−1884

quantitative yield. The free carbene moieties are then generated by deprotonation of the C2 hydrogen between the two lateral nitrogen atoms. Because of the extremely weak acidity at this position, a strong base such as potassium *tert*-butoxide or sodium hydride is required. The resulting NHC-appended polymer ligands are then stored in aprotic solvents under inert conditions (e.g., inside a glovebox). We have also prepared monodentate NHC-PEG ligands using the same PEG blocks introduced above and tested them as control coating and in the etching experiments discussed below. Additional details about the ligand synthesis and purification steps are provided in the Supporting Information.

The structures of the NHC-polymer and the intermediate compounds have been analytically confirmed by NMR spectroscopy (see Figure 1B−D). The spectrum collected from the imidazolium intermediate (APEIm-ium-PIMA-PEG) shows peaks at 7.85 and 9.24 ppm ascribed to the C4,5 and C2 protons in the heterocyclic ring along with a sharp peak at 1.45 ppm ascribed to the $-CH_2\underline{CH_3}$ group at the N3 position (see Figure 1C). The NMR spectrum collected after treatment of the APEIm-ium-PIMA-PEG intermediate with potassium *tert*-butoxide (in a THF solution) shows that the peaks at 7.85 and 1.45 ppm are preserved, while the one at 9.24 ppm has disappeared, indicating the successful transformation of the imidazolium groups to free carbene molecules (see Figure 1D); the resulting compound is termed NHC-PIMA-PEG. We should stress that potential interference from other groups (such as the amide and carbonyl alpha proton) in the polymer structures is unlikely because deprotonation of the amide or C−H alpha to carbonyls is less favorable. The pK_a associated with those groups is ∼26−30, while the pK_a of imidazolium is ∼21.[65,66] Integration of the proton peaks ascribed to the terminal methyl groups in PEG-OCH_3 (at 3.25 ppm) and the heterocyclic protons in the imidazole ring (at ∼6.9−7.7 ppm), in the spectrum acquired from APIm-PIMA-PEG, are compared to the integration of the broad peak at ∼0.9 ppm assigned to methyl groups of the PIMA backbone (∼39 × 2 per chain), yielding quantitative information about the stoichiometry of the polymer compound (see Figure 1B). The experimental values extracted from the integration data are in agreement with the nominal values (50% of APIm and 50% of PEG, expected from the precursor molar concentrations used), indicating a good control over the molar fraction of lateral moieties. Additional side-by-side characterization of the APEIm-ium-PIMA-PEG and NHC-PIMA-PEG has been performed using FTIR spectroscopy. The data show that the signatures ascribed to the C═O stretch peak (in COOH) at ∼1734 cm^{-1} (dashed line) have disappeared after base treatment, indicating the complete transformation of $-COO\underline{H}$ to $-COO\underline{K}$ groups along the polymer chain (see Figure S1).

Ligand Exchange. The newly prepared NHC-PIMA-PEG and NHC-PEG ligands have been tested for the coordination onto luminescent CdSe−ZnS QDs. The schematic in Figure 2A summarizes the protocol applied for ligating the QDs with NHC-PIMA-PEG. In a typical ligand exchange experiment with the polymer, excess free hydrophobic (native) ligands in the QD stock dispersion are first removed by precipitation using excess methanol. The pellet is then redispersed in $CHCl_3$ and mixed with NHC-PIMA-PEG solution (also in $CHCl_3$) and left to react for ∼10 min. This promotes the competitive substitution of the native ligands (a mixture of trioctylphosphine, TOP, trioctylphosphine oxide, TOPO, hexylphosphonic acid, HPA, and hexadecylamine, HDA) with the new ligands. Following removal of the displaced hydrophobic ligands using excess hexane combined with centrifugal precipitation, the resulting QD pellet is readily dispersed in aqueous media. The rapid NHC-promoted coordination of the polymer on the transition-metal-rich QD surfaces allows ligand substitution to be completed within 5−10 min. This rather short reaction time should be contrasted with those often required when using ligands that present "conventional" anchoring groups such as thiols, carboxyls, and even imidazoles, which necessitate reaction time anywhere between a few hours to overnight.[49,52,58] Ligation of NHC-PEG (monodentate) ligands onto the same QDs yields water-dispersible nanoparticles with limited colloidal stability. Additionally, a longer incubation time is needed, and the resulting dispersions are prone to aggregation often during processing (see Figure S2A).

To confirm that coordination of NHC-PIMA-PEG on the QDs is promoted by the NHC groups and not by the carboxyl or APEIm-ium groups, we performed a control experiment, where the hydrophobic QDs have been reacted with a solution of APEIm-ium-PIMA-PEG in $CHCl_3$. Irreversible precipitation of the QDs takes place either during mixing or within a few hours of ligand exchange and purification of the QDs, as shown in the Supporting Information (Figure S2B). This clearly proves that either imidazolium and carboxyl groups are incapable of competitively displacing the native cap or their interactions with the QDs are too weak to impart steric stability onto the nanocrystals. Additional details about the ligand substitution and phase transfer steps are provided in the Supporting Information.

We should note that performing the ligand substitution using THF as solvent, instead of chloroform, has yielded the same quality materials (see Figure S3). This proves that chloroform does not interfere with the NHC structure/nature. Indeed, $CHCl_3$ it is known to be a weak proton donor and does not exhibit self-dissociation.

Characterization of the Coordination Interactions. We have applied both ^1H and ^{13}C NMR spectroscopy and TEM characterization to gain insights into the nature of the coordination interactions and binding of the NHC ligands onto the ZnS-overcoated QD surfaces.

^1H NMR Characterization. Here, we analyze changes in the ^1H NMR spectra collected from QD dispersions before and after cap exchange, specifically focusing on a few proton signatures already identified above for the pure ligands. Figure 2 shows a side-by-side comparison between the ^1H NMR spectra collected from hydrophobic QDs in $CDCl_3$ (Figure 2B) and the same QDs after ligand exchange with the polymer, dispersed in D_2O (Figure 2C); water suppression has been applied to the spectrum acquired from the hydrophilic sample. The spectrum of the hydrophobic QDs shows only signatures limited to the range at ∼0.5−1.75 ppm, which are ascribed to the native ligands (namely, a mixture of TOP, TOPO, HDA, and HPA), in agreement with the data reported by our group for core−shell nanocrystals.[67] Those signatures are absent from the spectrum of the NHC-PIMA-PEG-QD sample (Figure 2C), which shows sharp peaks ascribed to the protons of the terminal methoxy at ∼3.3 ppm and the PEG block at ∼3.6 ppm. Additionally, a weak and broad peak at ∼0.9−1 ppm ascribed to the dimethyl protons of the PIMA chain is present.[58] We should note that once the polymer-QDs are exposed to water, the NMR spectrum acquired without water suppression from the polymer-QDs in D_2O shows the presence

https://dx.doi.org/10.1021/jacs.0c10592
J. Am. Chem. Soc. 2021, 143, 1873−1884

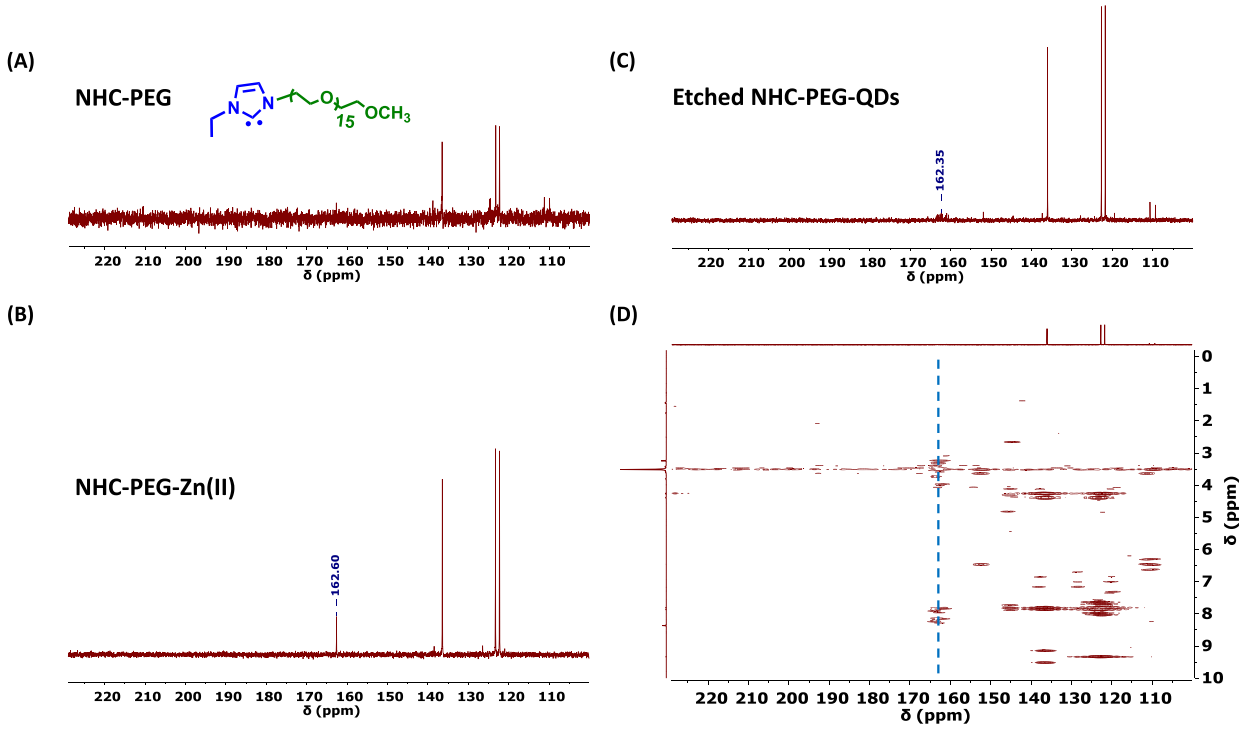

Figure 3. (A) ^{13}C NMR spectrum of NHC-PEG molecules. (B) ^{13}C NMR spectrum of NHC-PEG-Zn(II) complexes. The peak at ∼162.3 ppm is ascribed to the carbene carbon. (C, D) 1-D ^{13}C NMR along with the 2-D HMBC spectrum correlating the ^{1}H and ^{13}C signatures acquired for the QD sample under etching conditions using excess NHC-PEG ligands. The signal at ∼162.3 ppm proves the presence of carbene-Zn(II) complexes. Deuterated DMSO is used for all samples.

of weak signature at 9.24 ppm ascribed to the acidic proton along with the other two protons in the imidazole ring (see Figure S4). This indicates that a fraction of the C−H bonds at the C2 carbon have re-formed in hydrophilic media. We infer from integration of those peaks that ∼25% of the total NHC molecules in the sample have reversed back to imidazolium. However, this does not alter the colloidal integrity of the NHC-polymer-QDs in water, as we anticipate that the remaining intact groups (∼14−15 NHC per ligand) would still promote strong binding onto the NP surfaces.

Further proof of the NHC-polymer coordination on the QD surfaces has relied on DOSY NMR spectroscopy, where changes in the diffusion coefficient of the ligand protons are probed after coordination on the nanocrystals.[68] This technique has gained much interest for use to characterize the surface coating of various nanocolloids.[67−70] It has also been shown to provide reliable data on the diffusion coefficient of nanometer size solutes (e.g., nanocrystals), where the ubiquitous dynamic light scattering (DLS) technique tends to fail because of very weak scattering laser signals.[68] DOSY NMR relies on the application of two RF pulses carefully intercalated between two identical magnetic field gradient pulses, G_z, applied along the z-axis. The first RF 90° pulse is followed by a defocusing magnetic field gradient, and the second RF 180° pulse is followed by a second field gradient that achieves refocusing of the collective spin precession and recovery of the magnetization induction signal. Recovery of the signal is, however, strongly affected by the Brownian diffusion of the spin nuclei associated with the solute nanocrystals. The signal attenuation can be described by using the Stejskal−Tanner equation:[68,71]

$$I = I(G_z = 0)\mathrm{e}^{-D\gamma^2 G_z^2 \delta^2(\Delta-(\delta/3))} \quad (1)$$

where D is the diffusion coefficient, γ designates the gyromagnetic ratio of ^{1}H, G_z is the magnetic field gradient strength (applied during the pulse), Δ is the diffusion time (separating the two gradients pulses), and δ is the magnetic field gradient pulse duration.

Figure 2D shows the normalized magnetization intensity versus G_z^2 graphed in a semilog plot, acquired from dispersion of the NHC-polymer QDs and a solution of the polymer alone. The methoxy and ethylene oxide protons are used to track the signal attenuation. Figure 2E shows the corresponding DOSY contour spectra. Clearly, both plots show that there are two distinct diffusion coefficients extracted for the NMR data: one ascribed to the NHC-PIMA-PEG-QDs ($D \cong 2.18 \times 10^{-11}$ m^2/s) and the other ascribed to the free polymer ligands ($D \cong 6.91 \times 10^{-11}$ m^2/s). The smaller diffusion coefficient measured for the NHC-polymer-QDs, compared to the one for the polymer sample, indicates that only surface-bound ligands are detected in the QD sample. We note that the DOSY contour spectra also show a much faster diffusion coefficient at ∼4.7 ppm, which is ascribed to H_2O impurities in the D_2O solvent.[68] From the diffusion coefficient we can extract estimates for the hydrodynamic size using the Stokes−Einstein equation:[72]

$$R_H = \frac{k_B T}{6\pi\eta D} \quad (2)$$

where k_B is the Boltzmann constant, T is the temperature, and η is the viscosity of the medium. We extract $R_H \sim 3.1$ nm for the free ligands and $R_H \sim 9.8$ nm for the NHC-PIMA-PEG-QDs; these results are in good agreement with data acquired for other PEGylated, PIMA-based polymer ligands with lipoic acid anchoring motifs.[68,73] These data combined indicate that

https://dx.doi.org/10.1021/jacs.0c10592
J. Am. Chem. Soc. 2021, 143, 1873−1884

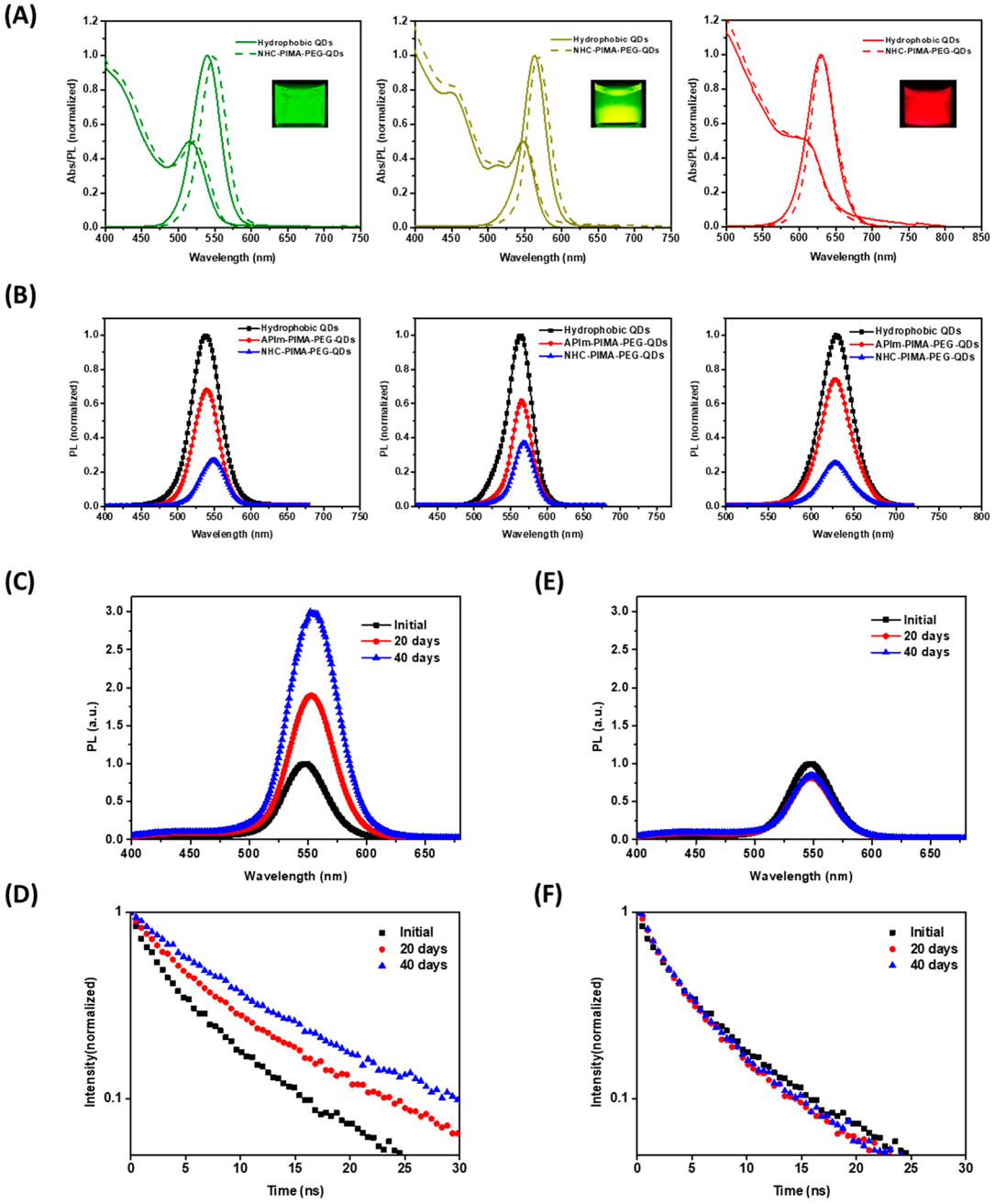

Figure 4. (A) Absorption and emission spectra collected from dispersions of green QDs, yellow QDs, and red QDs before and after ligand exchange. The green and yellow QDs were excited at 350 nm, while the red QDs were excited at 390 nm. The insets are the fluorescent images of aqueous QD dispersions collected under a UV lamp. (B) Side-by-side PL spectra acquired from dispersions of QDs with various coating, i.e., hydrophobic (TOP/TOPO/HPA-coated) along with hydrophilic APIm-PIMA-PEG-coated or NHC-PIMA-PEG-coated. (C, D) Time progression of the PL profiles collected from dispersions of NHC-PIMA-PEG-QDs in DI water stored under room light exposure along with the corresponding time-resolved PL decay profiles. (E, F) Time progression of PL spectra acquired from the same NHC-PIMA-PEG-QDs stored in the dark along with the corresponding PL decay profiles.

the polymer ligands are strongly bound to the QD surfaces, and the overall QD−ligand nanocolloids are compact in size.

We have further collected additional size measurements focusing on the inorganic nanocrystal cores using high-angle annular dark-field scanning transmission electron microscopy (HAADF-STEM) applied to QDs before and after ligand substitution with the polymer ligands (see Figure 2, panels F and G). The sizes acquired from both sets of QDs are essentially the same, which implies that under the conditions used there is no measurable etching of the QD surfaces. We should also note that the contrast of the QD cores in the TEM micrograph acquired from the NHC-polymer-coated QDs is lower than that measured for the hydrophobic samples—a result attributed to the viscous nature of the polymer coating. The smaller radii measured from TEM compared to the hydrodynamic radii collected from DOSY NMR reflect the difference in the physical definition and meaning of those sizes. R_H accounts for the contribution from the surface ligands due to hydrodynamic interactions, while TEM probes only the inorganic cores.

https://dx.doi.org/10.1021/jacs.0c10592
J. Am. Chem. Soc. 2021, 143, 1873−1884

^{13}C NMR Characterization. We applied ^{13}C NMR spectroscopy to gain further insight into the exact nature of the coordination interactions between the NHC groups and the ZnS-rich QD surfaces. It has been reported that upon carbene formation the ^{13}C chemical shift of the C2 carbon in the NHC ring can undergo a downfield shift toward 180−220 ppm.[74] Furthermore, that shift changes when NHC-to-metal complexation takes place.[75,76] However, we have found that detection of this ^{13}C signal is very difficult for NHC groups attached to our polymer ligand. Similar observations have been reported for other NHC-modified polymer by Thomas and coworkers.[77] Such result can be attributed to two combined factors: (1) The low natural abundance of the ^{13}C isotope (∼1%) yields rather weak NMR signals. (2) The tumbling dynamics of the NHC groups are much slower when these moieties are attached to a polymer chain, and they become even slower when the ligands are QD-bound.

To circumvent these constraints, we used NHC-PEG monomer coating instead, but under strong etching conditions; the structure of NHC-PEG is provided in Figure 3. The NHC-PEG ligands share some of the chemical features of the polymer (both have the same PEG-OMe) but tend to exhibit more pronounced NMR signal due to their lower molecular weight and faster dynamics in solution. In addition, we performed the ligand substitution of the QDs using a molar excess NHC-PEG that is much larger than those used for the phase transfer (∼10−20-fold higher) experiments discussed above. Such conditions can promote surface etching and even dissolution of the nanocrystals. This approach is based on two experimental observations: (1) Excess NHC molecules have been reported to etch metallic nanocrystals.[78,79] (2) Dispersions of nanocrystals under etching conditions yield increased NMR signal, compared to those prepared under normal conditions, due to the presence of metal−ligand complexes.[80]

We performed 1-D ^{13}C NMR and/or heteronuclear multiple bond correlation (HMBC) NMR spectroscopy experiments for a series of reaction mixtures, namely NHC-PEG alone, etched NHC-PEG-QDs, and NHC-PEG-Zn(II) generated by reacting NHC-PEG molecules with $ZnCl_2$ in solution, using either 600 or 700 MHz NMR instruments. As shown in Figure 3A, the NHC-PEG solution does not show any measurable downfield signal beyond 137 ppm. However, the HMBC spectrum collected from the same NHC-PEG solution shows a signature at (211, 4.4) ppm, correlating C2 to the protons of the ethyl coupled to N3 on the ring; additional details are provided in Figure S5. In comparison, a solution of NHC-PEG reacting with the molecular Zn(II) complex shows a well-defined new feature at ∼163.2 ppm, which we attribute to the C−Zn anticipated for the NHC reaction with Zn ions resulting in NHC-Zn complex formation (see Figure 3B). Additionally, a feature (though weaker) at the same chemical shift is measured for the etched NHC-PEG-QD sample, which provides proof for the formation of NHC−Zn bonds with the Zn-rich shell of the QDs (see Figure 3C). To further confirm the existence of this peak, HMBC NMR spectroscopy was applied to the NHC-etched QD sample.[22] The HMBC spectrum shows a correlation between the C2 carbon atom and hydrogens in the ethyl chain at N3 which are a few bonds away (see Figure 3A,D). These results confirm the existence of the C2−Zn binding in the NHC-PEG-QD sample, which allows us to conclude that our new stabilizing ligands bind onto the QDs via carbene-Zn coordination.[74,76] The corresponding enlarged 1-D ^1H NMR spectrum is provided in Figure S6.

Optical Characterization and Colloidal Stability Test.

Optical Characterization. Having confirmed that coordination onto the QD surfaces is driven by NHC-Zn(II) complexation, we now proceed to characterize the photophysical properties of the NHC-polymer-QD dispersions. Figure 4A shows the normalized UV−vis absorption and fluorescence spectra, acquired from three representative sets of QDs, before (TOP/TOPO/HPA-capped) and after ligand substitution with NHC-PIMA-PEG. Data show that overall the optical integrity of the nanocrystals is preserved. Nonetheless, a slight size-dependent red-shift in the absorption band edge and fluorescence peak location is measured: green QDs (shift ∼8 nm), yellow QDs (shift ∼5 nm), and red QDs (shift ∼1 nm). The reported shifts represent averages of values extracted from absorption and photoemission data collected from freshly prepared samples. Figure 4B shows the superposed PL spectra collected from green, yellow, and red QDs surface stabilized with the native cap, APIm-PIMA-PEG or NHC-PIMA-PEG ligands. Here, APIm-PIMA-PEG-coated QDs are used as an additional control because such imidazole-presenting ligands were shown to stabilize CdSe-ZnS QDs, while maintaining high fluorescence emission, which is close to that measured for the starting hydrophobic nanocrystals.[58] Data show that indeed imidazole-presenting polymer coating yields substantially higher emission than those measured for NHC-polymer coating. In addition, size-dependent red-shifts can be identified when comparing the emission spectra acquired from NHC-PIMA-PEG-QDs side-by-side with APIm-PIMA-PEG-QDs or the native hydrophobic QDs. The data in Figure 4A,B show that NHC-polymer coating imposes ∼70−75% loss in the PL intensity compared to ∼25−30% loss measured for the APIm-PIMA-PEG-coated QDs (for the three sets of QDs tested). They also show that only the NHC coordination generated a color-dependent red-shift in the emission/absorption compared to the native nanocrystals, while imidazole coordination does not. The fluorescence properties of the NHC-polymer-QD dispersions (green-emitting) in DI water were evaluated following storage in the dark (at 4 °C in the fridge) or under room light and temperature conditions. Figure 4C−F shows a summary of the fluorescence data along with the PL lifetime profiles for both sets of dispersions tracked over a period of 40 days. We find that exposure to room light induces an increase in the PL intensity, coupled with lengthening of the fluorescence lifetime and a slight red-shift in the emission peak. In comparison, no change in either the PL intensity or the lifetime was measured for the dispersions stored in the dark. No such effects have been measured for QDs capped with lipoic acid or/an imidazole anchor when stored under light exposure.[58,73]

The red-shift in the absorption and emission properties of the NHC-polymer-coated QDs (shown in Figure 4A,B) is consistent with recent results reported by Weiss and coauthors for core only QDs mixed with NHC-containing molecules.[81] They reported that the absorption band edge can exhibit a red-shift that reaches ∼106 meV.[81] Our largest shift, measured for the green QDs, is ∼33 meV (for a freshly prepared dispersion) but reaches ∼50 meV after 40 days of storage under light exposure; it is smaller than their largest value. If we use the rationale proposed by Weiss's group, namely that delocalization of the photoinduced excitons (generated within the inorganic cores) into the carbene-rich coating molecules, we

https://dx.doi.org/10.1021/jacs.0c10592
J. Am. Chem. Soc. 2021, 143, 1873−1884

can then infer that the presence of a ZnS shell reduces such a delocalization process. Indeed, the original rationale for overcoating the QD cores to enhance the photoemission, by using wider band gap shell materials, was aimed at promoting better confinement of the exciton within the cores and increasing the fluorescence radiative recombination rates. Thus, in our case the ZnS shell provides a protective shield, which reduces the degree of exciton delocalization into the carbene-rich organic shell. We may add that the core only QDs used by Weiss exhibited little to no PL signal, while our materials still produced strong fluorescence properties, albeit lower than the native hydrophobic or hydrophilic APIm-PIMA-PEG-coated QDs.

The enhancement in the PL properties of NHC-polymer-QDs with storage time under room light exposure is an interesting feature and agrees with several studies showing that irradiation of various surface-stabilized quantum dots and quantum rods yields a sizable increase in the PL intensity.[82,83] They tend to occur with dispersions that have rather reduced emission properties (low quantum yield), such as is the case with our NHC-stabilized nanocrystals. We note that the measured changes in the fluorescence intensity with storage are commensurate with those measured for the lifetimes. The fluorescence quantum yield (QY) as defined depends on the radiative and nonradiative exciton decay pathways:[84]

$$\mathrm{QY} = \frac{k_\mathrm{r}}{k_\mathrm{r} + k_\mathrm{nr}} \tag{3}$$

where k_r and k_nr respectively designate the radiative and nonradiative decay rates. To gain insights into how storage under light exposure affects the fluorescence data, we compare the relative fluorescence intensity measured for the dispersion with days of storage (F_d), since the data were collected from the same sample at day 1, day 20, and day 40 under the same conditions. We also assume that only k_nr is affected by the light exposure. This allows us to write that at day dx:

$$\frac{F_{dx}}{F_{d1}} = \frac{\mathrm{QY}_{dx}}{\mathrm{QY}_{d1}} = \frac{\frac{k_{r-dx}}{k_{r-dx}+k_{nr-dx}}}{\frac{k_{r-d1}}{k_{r-d1}+k_{nr-d1}}} = \frac{k_{r-d1}+k_{nr-d1}}{k_{r-dx}+k_{nr-dx}} = \frac{\tau_{dx}}{\tau_{d1}} \tag{4}$$

where we replaced $\frac{1}{k_\mathrm{r}+k_\mathrm{nr}}$ with the PL lifetime, τ, extracted from the experimental data (see Table 1). From the fluorescence and lifetime data we estimate that $\frac{F_{d20}}{F_{d1}} \sim 1.9$ while $\frac{\tau_{d20}}{\tau_{d1}} \sim 2.0$ and $\frac{F_{d40}}{F_{d1}} \sim 3.0$ and $\frac{\tau_{d40}}{\tau_{d1}} \sim 2.8$. This agreement supports our assumption and implies that light exposure activates some of the shallow surface traps which are the main pathways for nonradiative exciton recombination.[82,83] This ultimately results in a pronounced recovery of the fluorescence intensity under room light exposure (see data shown in Figure 4C,D).

Table 1. PL Intensity and Time-Resolved Lifetime Data for QD Samples Stored under Light Exposure

storage time	PL intensity (normalized)	PL lifetime (ns)
day 1	1	4.17
day 20	1.9	8.51
day 40	3.0	11.80

Colloidal Stability Tests. This test has focused on tracking the long-term colloidal stability of several dispersions of luminescent QDs surface-stabilized with the new NHC-polymer ligands. These include dispersions in 20 mM phosphate buffers at pH ranging from 3 to 12, buffer containing 1 M NaCl, and dispersions of QDs mixed with 0.5 M dithiothreitol (DTT). We also characterized the gel mobility of the QDs at the same pHs and when mixed with serum bovine albumin (BSA) in large excess.[85,86] Dispersions in DI water were used as control samples.

These dispersions have been stored under room temperature and light exposure conditions, and fluorescent images were periodically collected from the various samples, while illuminated with a hand-held UV lamp, by using a camera (Nikon D3300). Figure 5A,B shows that the dispersions stayed homogeneous and aggregate-free over a period of at least 6 months. The images also show that the brightness of the samples visibly increased with time (e.g., compare images from fresh samples and 6 months of storage), a result that is consistent with the data shown in Figure 4C. However, dispersions at pH 3 exhibit a pronounced reduction of fluorescence with time, but without losing their colloidal nature and with no sign of aggregation. This may be attributed to partial protonation of the anchoring NHCs along the polymer ligand under acidic conditions. The protonated imidazolium groups exhibit weakened coordination of the ligands onto the nanosized QDs, resulting in more exposed surfaces and loss in PL. Figure 5C,D shows gel electrophoresis images acquired from agarose gels loaded with the various QD dispersions described above. The gel bands are imaged, in the fluorescence mode, by using a UV lamp for excitation. Tight fluorescent bands that migrate toward the anode, with the same mobility shift, have been measured for all samples. The shift toward to the anode is attributed to the net negative charge of the QD surfaces because of the presence of carboxyl (or carboxylate) groups along the NHC-polymer backbone.[58] Additionally, narrow bands and identical mobility shifts are observed for all wells, implying that monodisperse nanocolloids of NHC-PIMA-PEG-QDs characterize the dispersions for all pHs. These long-term colloidal stability data combined with the gel electrophoresis experiments indicate that the NHC-polymer coating promotes effective steric stabilization of the QDs under a variety of conditions (except pH 3). In addition, the absence of any change in the mobility shift measured for the dispersion containing excess BSA indicates that the PEG-rich coating indeed prevents nonspecific interactions and corona formation around the QDs.[87,88] This result agrees with previous reports investigating QDs capped with other PIMA-based ligands modified with different coordinating groups (e.g., lipoic acid or phosphonic acid).[52,58] Finally, we would like to add that the NHC-polymer coating imparts colloidal stability while preserving the fluorescent nature of the QDs dispersed in water mixed with H_2O_2 (up to 250 mM) and QD dispersions in organic solvents such as $CHCl_3$ and acetone; they also preserve the fluorescence properties of the nanocrystals as dried pellets (see Figure S7).

CONCLUSION

In this report we have demonstrated that ligands presenting N-heterocyclic carbene (NHC) groups can rapidly react with and coordinate onto luminescent CdSe−ZnS core−shell quantum dots. Furthermore, we found that installing multiple NHC

https://dx.doi.org/10.1021/jacs.0c10592
J. Am. Chem. Soc. 2021, 143, 1873−1884

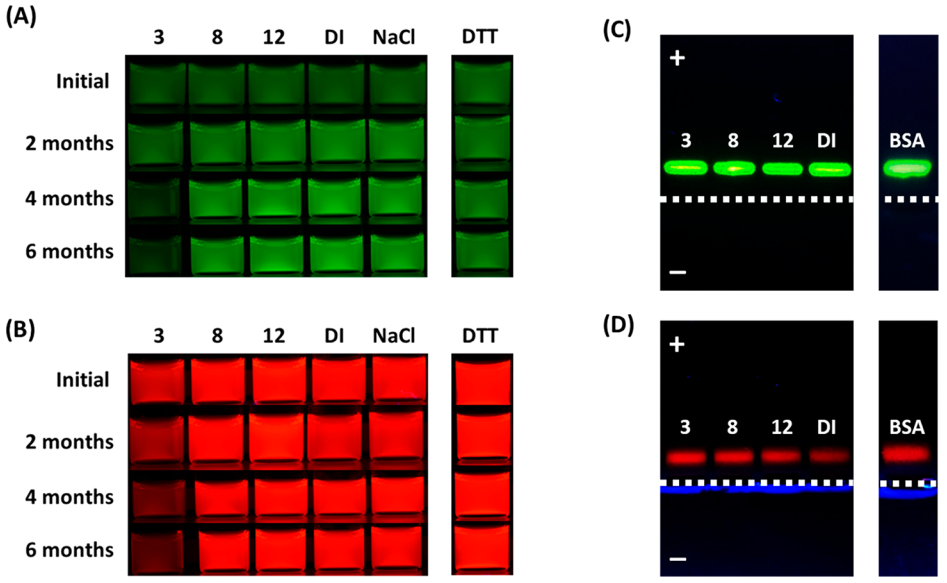

Figure 5. (A, B) Colloidal stability tests applied to green- and red-emitting NHC-PIMA-PEG-QDs. Dispersions in buffers at pH 3, 8, and 12 in DI water, in 1 M NaCl, and in 0.5 M DTT. Images were collected by using a Nikon D3300 camera. Samples were UV illuminated by using a hand-held UV lamp. (C, D) Gel electrophoresis images of green- and red-emitting NHC-PIMA-PEG-QDs, run on 0.6% agarose gel by using Tris borate EDTA buffer for 30 min under a voltage of 5.5 V/cm. The wells on the right was loaded with dispersions of QDs mixed with BSA and preincubated for 1 h. The dashed lines in panels C and D designate the loading wells. The images were collected under fluorescence mode as described for the stability data.

groups and hydrophilic moieties in the ligand structure promotes high affinity of the resulting QDs to water media. This is achieved by exploiting the unique advantages of the nucleophilic addition reaction between anhydride rings and amine-R nucleophiles, which is highly efficient, provides controllable stoichiometry, and affords the ability to combine different functional groups into one single ligand. In particular, we have shown that polymer ligands, presenting several NHC groups and multiple poly(ethylene glycol) blocks, promote long-term colloidal and photophysical stability of the QDs in buffer media, while preventing nonspecific interactions with bovine serum albumin (BSA). The rapid coordination (requiring ∼5−10 min of mixing) reflects the nature of the NHC groups as soft Lewis base with strong interactions with transition metals ions (soft/borderline Lewis acid). The generation of the carbene groups and the complete substitution of the hydrophobic coating with the new NHC-based ligands have been verified by using a combination of 1-D ^{1}H NMR and 2-D DOSY NMR spectroscopy. In addition, we employed 1-D ^{13}C NMR and 2-D heteronuclear multiple bond correlation (HMBC) NMR spectroscopy to identify the presence of carbene−Zn complexes, further confirming the coordination of the carbene onto the Zn-rich QD surfaces. We also found that the new NHC coating introduces subtle changes to the optical and spectroscopic properties of the nanocrystals. These include a size-dependent red-shift of the absorption and emission spectra and a pronounced increase in the fluorescence intensity when the samples are stored under white light exposure. We note that these ligands can also stabilize Au nanocolloids in buffer media.[89] These results combined expand the use of NHC molecules to stabilize nanocrystals with transition-metal-rich surfaces in both organic and hydrophilic media. They bode well for the integration of these newly coated colloids in various applications.

■ ASSOCIATED CONTENT

Supporting Information

The Supporting Information is available free of charge at https://pubs.acs.org/doi/10.1021/jacs.0c10592.

Materials, instrumentation, ligand synthesis, ligand exchange, additional NMR and FTIR spectra, long-term stability of NHC-stabilized QDs dispersed in organic solvents as well as dried pellets (PDF)

■ AUTHOR INFORMATION

Corresponding Author

Hedi Mattoussi − *Department of Chemistry and Biochemistry, Florida State University, Tallahassee, Florida 32306, United States*; orcid.org/0000-0002-6511-9323; Email: mattoussi@fsu.edu

Authors

Liang Du − *Department of Chemistry and Biochemistry, Florida State University, Tallahassee, Florida 32306, United States*

Neda Arabzadeh Nosratabad − *Department of Chemistry and Biochemistry, Florida State University, Tallahassee, Florida 32306, United States*

Zhicheng Jin − *Department of Chemistry and Biochemistry, Florida State University, Tallahassee, Florida 32306, United States*

Chengqi Zhang − *Department of Chemistry and Biochemistry, Florida State University, Tallahassee, Florida 32306, United States*

Sisi Wang − *Department of Chemistry and Biochemistry, Florida State University, Tallahassee, Florida 32306, United States*

Banghao Chen − *Department of Chemistry and Biochemistry, Florida State University, Tallahassee, Florida 32306, United States*

https://dx.doi.org/10.1021/jacs.0c10592
J. Am. Chem. Soc. 2021, 143, 1873−1884

Complete contact information is available at:
https://pubs.acs.org/10.1021/jacs.0c10592

Notes

The authors declare no competing financial interest.

■ ACKNOWLEDGMENTS

The authors thank FSU, the National Science Foundation (NSF-CHE, Grant #1508501 and #2005079), AFOSR (Grant #FA9550-18-1-0144), and Asahi-Kasei Inc. for financial support. The TEM work was performed at the National High Magnetic Field Laboratory, which is supported by National Science Foundation Cooperative Agreement No. DMR-1644779 and the State of Florida. We also thank Dr. Yan Xin for the assistance with the TEM experiments.

■ REFERENCES

(1) Arduengo, A. J.; Harlow, R. L.; Kline, M. A stable crystalline carbene. *J. Am. Chem. Soc.* **1991**, *113*, 361−363.
(2) Hopkinson, M. N.; Richter, C.; Schedler, M.; Glorius, F. An overview of N-heterocyclic carbenes. *Nature* **2014**, *510*, 485−496.
(3) Kantchev, E. A. B.; O'Brien, C. J.; Organ, M. G. Palladium Complexes of N-Heterocyclic Carbenes as Catalysts for Cross-Coupling Reactions—A Synthetic Chemist's Perspective. *Angew. Chem., Int. Ed.* **2007**, *46*, 2768−2813.
(4) Fortman, G. C.; Nolan, S. P. N-Heterocyclic carbene (NHC) ligands and palladium in homogeneous cross-coupling catalysis: a perfect union. *Chem. Soc. Rev.* **2011**, *40*, 5151−5169.
(5) Valente, C.; Çalimsiz, S.; Hoi, K. H.; Mallik, D.; Sayah, M.; Organ, M. G. The Development of Bulky Palladium NHC Complexes for the Most-Challenging Cross-Coupling Reactions. *Angew. Chem., Int. Ed.* **2012**, *51*, 3314−3332.
(6) Samojłowicz, C.; Bieniek, M.; Grela, K. Ruthenium-Based Olefin Metathesis Catalysts Bearing N-Heterocyclic Carbene Ligands. *Chem. Rev.* **2009**, *109*, 3708−3742.
(7) Endo, K.; Grubbs, R. H. Chelated Ruthenium Catalysts for Z-Selective Olefin Metathesis. *J. Am. Chem. Soc.* **2011**, *133*, 8525−8527.
(8) Bayón Castañón, E. Water-insoluble and water-soluble NHC complexes and their applications in hydrogenation reactions. Ph.D. Thesis. Technische Universität München, Aug 2018.
(9) Zou, T.; Lok, C.-N.; Wan, P.-K.; Zhang, Z.-F.; Fung, S.-K.; Che, C.-M. Anticancer metal-N-heterocyclic carbene complexes of gold, platinum and palladium. *Curr. Opin. Chem. Biol.* **2018**, *43*, 30−36.
(10) Hickey, J. L.; Ruhayel, R. A.; Barnard, P. J.; Baker, M. V.; Berners-Price, S. J.; Filipovska, A. Mitochondria-Targeted Chemotherapeutics: The Rational Design of Gold(I) N-Heterocyclic Carbene Complexes That are Selectively Toxic to Cancer Cells and Target Protein Selenols in Preference to Thiols. *J. Am. Chem. Soc.* **2008**, *130*, 12570−12571.
(11) Pratesi, A.; Gabbiani, C.; Michelucci, E.; Ginanneschi, M.; Papini, A. M.; Rubbiani, R.; Ott, I.; Messori, L. Insights on the mechanism of thioredoxin reductase inhibition by Gold N-heterocyclic carbene compounds using the synthetic linear Selenocysteine containing C-terminal peptide hTrxR(488−499): An ESI-MS investigation. *J. Inorg. Biochem.* **2014**, *136*, 161−169.
(12) Dos Santos, H. F.; Vieira, M. A.; Sánchez Delgado, G. Y.; Paschoal, D. Ligand Exchange Reaction of Au(I) R-N-Heterocyclic Carbene Complexes with Cysteine. *J. Phys. Chem. A* **2016**, *120*, 2250−2259.
(13) Wai-Yin Sun, R.; Lok-Fung Chow, A.; Li, X.-H.; Yan, J. J.; Sin-Yin Chui, S.; Che, C.-M. Luminescent cyclometalated platinum(II) complexes containing N-heterocyclic carbene ligands with potent in vitro and in vivo anti-cancer properties accumulate in cytoplasmic structures of cancer cells. *Chem. Sci.* **2011**, *2*, 728−736.
(14) Li, K.; Zou, T.; Chen, Y.; Guan, X.; Che, C.-M. Pincer-Type Platinum(II) Complexes Containing N-Heterocyclic Carbene (NHC) Ligand: Structures, Photophysical and Anion-Binding Properties, and Anticancer Activities. *Chem. - Eur. J.* **2015**, *21*, 7441−7453.
(15) Fong, T. T.-H.; Lok, C.-N.; Chung, C. Y.-S.; Fung, Y.-M. E.; Chow, P.-K.; Wan, P.-K.; Che, C.-M. Cyclometalated Palladium(II) N-Heterocyclic Carbene Complexes: Anticancer Agents for Potent In Vitro Cytotoxicity and In Vivo Tumor Growth Suppression. *Angew. Chem., Int. Ed.* **2016**, *55*, 11935−11939.
(16) Ray, S.; Mohan, R.; Singh, J. K.; Samantaray, M. K.; Shaikh, M. M.; Panda, D.; Ghosh, P. Anticancer and Antimicrobial Metallopharmaceutical Agents Based on Palladium, Gold, and Silver N-Heterocyclic Carbene Complexes. *J. Am. Chem. Soc.* **2007**, *129*, 15042−15053.
(17) Rühling, A.; Schaepe, K.; Rakers, L.; Vonhören, B.; Tegeder, P.; Ravoo, B. J.; Glorius, F. Modular Bidentate Hybrid NHC-Thioether Ligands for the Stabilization of Palladium Nanoparticles in Various Solvents. *Angew. Chem., Int. Ed.* **2016**, *55*, 5856−5860.
(18) Gonzalez-Galvez, D.; Lara, P.; Rivada-Wheelaghan, O.; Conejero, S.; Chaudret, B.; Philippot, K.; van Leeuwen, P. W. N. M. NHC-stabilized ruthenium nanoparticles as new catalysts for the hydrogenation of aromatics. *Catal. Sci. Technol.* **2013**, *3*, 99−105.
(19) MacLeod, M. J.; Goodman, A. J.; Ye, H.-Z.; Nguyen, H. V. T.; Van Voorhis, T.; Johnson, J. A. Robust gold nanorods stabilized by bidentate N-heterocyclic-carbene−thiolate ligands. *Nat. Chem.* **2019**, *11*, 57−63.
(20) Man, R. W. Y.; Li, C.-H.; MacLean, M. W. A.; Zenkina, O. V.; Zamora, M. T.; Saunders, L. N.; Rousina-Webb, A.; Nambo, M.; Crudden, C. M. Ultrastable Gold Nanoparticles Modified by Bidentate N-Heterocyclic Carbene Ligands. *J. Am. Chem. Soc.* **2018**, *140*, 1576−1579.
(21) Möller, N.; Rühling, A.; Lamping, S.; Hellwig, T.; Fallnich, C.; Ravoo, B. J.; Glorius, F. Stabilization of High Oxidation State Upconversion Nanoparticles by N-Heterocyclic Carbenes. *Angew. Chem., Int. Ed.* **2017**, *56*, 4356−4360.
(22) Thanneeru, S.; Ayers, K. M.; Anuganti, M.; Zhang, L.; Kumar, C. V.; Ung, G.; He, J. N-Heterocyclic carbene-ended polymers as surface ligands of plasmonic metal nanoparticles. *J. Mater. Chem. C* **2020**, *8*, 2280−2288.
(23) Dagorne, S. Recent Developments on N-Heterocyclic Carbene Supported Zinc Complexes: Synthesis and Use in Catalysis. *Synthesis* **2018**, *50*, 3662−3670.
(24) Hines, M. A.; Guyot-Sionnest, P. Synthesis and characterization of strongly luminescing ZnS-Capped CdSe nanocrystals. *J. Phys. Chem.* **1996**, *100*, 468−471.
(25) Dabbousi, B. O.; RodriguezViejo, J.; Mikulec, F. V.; Heine, J. R.; Mattoussi, H.; Ober, R.; Jensen, K. F.; Bawendi, M. G. (CdSe)ZnS core-shell quantum dots: Synthesis and characterization of a size series of highly luminescent nanocrystallites. *J. Phys. Chem. B* **1997**, *101*, 9463−9475.
(26) Clapp, A. R.; Goldman, E. R.; Mattoussi, H. Capping of CdSe−ZnS quantum dots with DHLA and subsequent conjugation with proteins. *Nat. Protoc.* **2006**, *1*, 1258−1266.
(27) Chen, O.; Zhao, J.; Chauhan, V. P.; Cui, J.; Wong, C.; Harris, D. K.; Wei, H.; Han, H.-S.; Fukumura, D.; Jain, R. K.; Bawendi, M. G. Compact high-quality CdSe−CdS core−shell nanocrystals with narrow emission linewidths and suppressed blinking. *Nat. Mater.* **2013**, *12*, 445−451.
(28) Sun, Q.; Wang, Y. A.; Li, L. S.; Wang, D.; Zhu, T.; Xu, J.; Yang, C.; Li, Y. Bright, multicoloured light-emitting diodes based on quantum dots. *Nat. Photonics* **2007**, *1*, 717−722.
(29) Kovalenko, M. V.; Manna, L.; Cabot, A.; Hens, Z.; Talapin, D. V.; Kagan, C. R.; Klimov, V. I.; Rogach, A. L.; Reiss, P.; Milliron, D. J.; Guyot-Sionnnest, P.; Konstantatos, G.; Parak, W. J.; Hyeon, T.; Korgel, B. A.; Murray, C. B.; Heiss, W. Prospects of Nanoscience with Nanocrystals. *ACS Nano* **2015**, *9*, 1012−1057.
(30) Chuang, C.-H. M.; Brown, P. R.; Bulović, V.; Bawendi, M. G. Improved performance and stability in quantum dot solar cells through band alignment engineering. *Nat. Mater.* **2014**, *13*, 796−801.
(31) Sarkar, S.; Le, P.; Geng, J.; Liu, Y.; Han, Z.; Zahid, M. U.; Nall, D.; Youn, Y.; Selvin, P. R.; Smith, A. M. Short-Wave Infrared

Quantum Dots with Compact Sizes as Molecular Probes for Fluorescence Microscopy. *J. Am. Chem. Soc.* **2020**, *142*, 3449−3462.
(32) Etoc, F.; Balloul, E.; Vicario, C.; Normanno, D.; Liße, D.; Sittner, A.; Piehler, J.; Dahan, M.; Coppey, M. Non-specific interactions govern cytosolic diffusion of nanosized objects in mammalian cells. *Nat. Mater.* **2018**, *17*, 740−746.
(33) Wang, W.; Mattoussi, H. Engineering the Bio−Nano Interface Using a Multifunctional Coordinating Polymer Coating. *Acc. Chem. Res.* **2020**, *53*, 1124−1138.
(34) Michalet, X.; Pinaud, F. F.; Bentolila, L. A.; Tsay, J. M.; Doose, S.; Li, J. J.; Sundaresan, G.; Wu, A. M.; Gambhir, S. S.; Weiss, S. Quantum Dots for Live Cells, in Vivo Imaging, and Diagnostics. *Science* **2005**, *307* (5709), 538−544.
(35) Mattoussi, H.; Palui, G.; Na, H. B. Luminescent quantum dots as platforms for probing in vitro and in vivo biological processes. *Adv. Drug Delivery Rev.* **2012**, *64*, 138−166.
(36) Zhan, N. Q.; Palui, G.; Safi, M.; Ji, X.; Mattoussi, H. Multidentate Zwitterionic Ligands Provide Compact and Highly Biocompatible Quantum Dots. *J. Am. Chem. Soc.* **2013**, *135*, 13786−13795.
(37) Wang, W.; Ji, X.; Na, H. B.; Safi, M.; Smith, A.; Palui, G.; Perez, J. M.; Mattoussi, H. Design of a Multi-Dopamine-Modified Polymer Ligand Optimally Suited for Interfacing Magnetic Nanoparticles with Biological Systems. *Langmuir* **2014**, *30*, 6197−6208.
(38) Palui, G.; Aldeek, F.; Wang, W. T.; Mattoussi, H. Strategies for interfacing inorganic nanocrystals with biological systems based on polymer-coating. *Chem. Soc. Rev.* **2015**, *44*, 193−227.
(39) Mattoussi, H.; Mauro, J. M.; Goldman, E. R.; Anderson, G. P.; Sundar, V. C.; Mikulec, F. V.; Bawendi, M. G. Self-Assembly of CdSe−ZnS Quantum Dot Bioconjugates Using an Engineered Recombinant Protein. *J. Am. Chem. Soc.* **2000**, *122*, 12142−12150.
(40) Susumu, K.; Oh, E.; Delehanty, J. B.; Blanco-Canosa, J. B.; Johnson, B. J.; Jain, V.; Hervey, W. J.; Algar, W. R.; Boeneman, K.; Dawson, P. E.; Medintz, I. L. Multifunctional Compact Zwitterionic Ligands for Preparing Robust Biocompatible Semiconductor Quantum Dots and Gold Nanoparticles. *J. Am. Chem. Soc.* **2011**, *133*, 9480−9496.
(41) Wang, W.; Ji, X.; Du, L.; Mattoussi, H. Enhanced Colloidal Stability of Various Gold Nanostructures Using a Multicoordinating Polymer Coating. *J. Phys. Chem. C* **2017**, *121*, 22901−22913.
(42) Breshike, C. J.; Riskowski, R. A.; Strouse, G. F. Leaving Förster Resonance Energy Transfer Behind: Nanometal Surface Energy Transfer Predicts the Size-Enhanced Energy Coupling between a Metal Nanoparticle and an Emitting Dipole. *J. Phys. Chem. C* **2013**, *117*, 23942−23949.
(43) Oh, E.; Susumu, K.; Mäkinen, A. J.; Deschamps, J. R.; Huston, A. L.; Medintz, I. L. Colloidal Stability of Gold Nanoparticles Coated with Multithiol-Poly(ethylene glycol) Ligands: Importance of Structural Constraints of the Sulfur Anchoring Groups. *J. Phys. Chem. C* **2013**, *117*, 18947−18956.
(44) Yildiz, I.; McCaughan, B.; Cruickshank, S. F.; Callan, J. F.; Raymo, F. M. Biocompatible CdSe-ZnS Core-Shell Quantum Dots Coated with Hydrophilic Polythiols. *Langmuir* **2009**, *25*, 7090−7096.
(45) Giovanelli, E.; Muro, E.; Sitbon, G.; Hanafi, M.; Pons, T.; Dubertret, B.; Lequeux, N. Highly Enhanced Affinity of Multidentate versus Bidentate Zwitterionic Ligands for Long-Term Quantum Dot Bioimaging. *Langmuir* **2012**, *28*, 15177−15184.
(46) Wang, W.; Aldeek, F.; Ji, X.; Zeng, B.; Mattoussi, H. A multifunctional amphiphilic polymer as a platform for surface-functionalizing metallic and other inorganic nanostructures. *Faraday Discuss.* **2014**, *175*, 137−51.
(47) Han, H.-S.; Martin, J. D.; Lee, J.; Harris, D. K.; Fukumura, D.; Jain, R. K.; Bawendi, M. Spatial Charge Configuration Regulates Nanoparticle Transport and Binding Behavior In Vivo. *Angew. Chem., Int. Ed.* **2013**, *52*, 1414−1419.
(48) Xia, C.; Wang, W.; Du, L.; Rabouw, F. T.; van den Heuvel, D. J.; Gerritsen, H. C.; Mattoussi, H.; de Mello Donega, C. Förster Resonance Energy Transfer between Colloidal $CuInS_2$/ZnS Quantum Dots and Dark Quenchers. *J. Phys. Chem. C* **2020**, *124*, 1717−1731.
(49) Wang, W.; Ji, X.; Kapur, A.; Zhang, C.; Mattoussi, H. A Multifunctional Polymer Combining the Imidazole and Zwitterion Motifs as a Biocompatible Compact Coating for Quantum Dots. *J. Am. Chem. Soc.* **2015**, *137*, 14158−14172.
(50) Tasso, M.; Giovanelli, E.; Zala, D.; Bouccara, S.; Fragola, A.; Hanafi, M.; Lenkei, Z.; Pons, T.; Lequeux, N. Sulfobetaine−Vinylimidazole Block Copolymers: A Robust Quantum Dot Surface Chemistry Expanding Bioimaging's Horizons. *ACS Nano* **2015**, *9*, 11479−11489.
(51) Grazon, C.; Chern, M.; Ward, K.; Lecommandoux, S.; Grinstaff, M. W.; Dennis, A. M. A versatile and accessible polymer coating for functionalizable zwitterionic quantum dots with high DNA grafting efficiency. *Chem. Commun.* **2019**, *55*, 11067−11070.
(52) Du, L.; Wang, W.; Zhang, C.; Jin, Z.; Palui, G.; Mattoussi, H. A Versatile Coordinating Ligand for Coating Semiconductor, Metal, and Metal Oxide Nanocrystals. *Chem. Mater.* **2018**, *30*, 7269−7279.
(53) Holland, G. P.; Sharma, R.; Agola, J. O.; Amin, S.; Solomon, V. C.; Singh, P.; Buttry, D. A.; Yarger, J. L. NMR Characterization of Phosphonic Acid Capped SnO_2 Nanoparticles. *Chem. Mater.* **2007**, *19*, 2519−2526.
(54) Cao, P.; Tong, L.; Hou, Y.; Zhao, G.; Guerin, G.; Winnik, M. A.; Nitz, M. Improving Lanthanide Nanocrystal Colloidal Stability in Competitive Aqueous Buffer Solutions using Multivalent PEG-Phosphonate Ligands. *Langmuir* **2012**, *28*, 12861−12870.
(55) Chanteau, B.; Fresnais, J.; Berret, J. F. Electrosteric Enhanced Stability of Functional Sub-10 nm Cerium and Iron Oxide Particles in Cell Culture Medium. *Langmuir* **2009**, *25*, 9064−9070.
(56) Calzada, R.; Thompson, C. M.; Westmoreland, D. E.; Edme, K.; Weiss, E. A. Organic-to-Aqueous Phase Transfer of Cadmium Chalcogenide Quantum Dots Using a Sulfur-Free Ligand for Enhanced Photoluminescence and Oxidative Stability. *Chem. Mater.* **2016**, *28*, 6716−6723.
(57) Malhotra, K.; Fuku, R.; Chan, T. S.; Kraljevic, N.; Sedighi, A.; Piunno, P. A. E.; Krull, U. J. Bisphosphonate Polymeric Ligands on Inorganic Nanoparticles. *Chem. Mater.* **2020**, *32*, 4002−4012.
(58) Wang, W.; Kapur, A.; Ji, X.; Safi, M.; Palui, G.; Palomo, V.; Dawson, P. E.; Mattoussi, H. Photoligation of an Amphiphilic Polymer with Mixed Coordination Provides Compact and Reactive Quantum Dots. *J. Am. Chem. Soc.* **2015**, *137*, 5438−5451.
(59) Jin, Z.; Du, L.; Zhang, C.; Sugiyama, Y.; Wang, W.; Palui, G.; Wang, S.; Mattoussi, H. Modification of Poly(maleic anhydride)-Based Polymers with H_2N−R Nucleophiles: Addition or Substitution Reaction? *Bioconjugate Chem.* **2019**, *30*, 871−880.
(60) Stewart, M. H.; Susumu, K.; Mei, B. C.; Medintz, I. L.; Delehanty, J. B.; Blanco-Canosa, J. B.; Dawson, P. E.; Mattoussi, H. Multidentate Poly(ethylene glycol) Ligands Provide Colloidal Stability to Semiconductor and Metallic Nanocrystals in Extreme Conditions. *J. Am. Chem. Soc.* **2010**, *132*, 9804−9813.
(61) Liong, M.; Shao, H.; Haun, J. B.; Lee, H.; Weissleder, R. Carboxymethylated Polyvinyl Alcohol Stabilizes Doped Ferrofluids for Biological Applications. *Adv. Mater.* **2010**, *22*, 5168−5172.
(62) Shukoor, M. I.; Natalio, F.; Ksenofontov, V.; Tahir, M. N.; Eberhardt, M.; Theato, P.; Schröder, H. C.; Müller, W. E. G.; Tremel, W. Double-Stranded RNA Polyinosinic−Polycytidylic Acid Immobilized onto γ-Fe_2O_3 Nanoparticles by Using a Multifunctional Polymeric Linker. *Small* **2007**, *3*, 1374−1378.
(63) Wang, S.; Du, L.; Jin, Z.; Xin, Y.; Mattoussi, H. Enhanced Stabilization and Easy Phase Transfer of CsPbBr3 Perovskite Quantum Dots Promoted by High-Affinity Polyzwitterionic Ligands. *J. Am. Chem. Soc.* **2020**, *142*, 12669−12680.
(64) Mei, B. C.; Susumu, K.; Medintz, I. L.; Delehanty, J. B.; Mountziaris, T. J.; Mattoussi, H. Modular poly(ethylene glycol) ligands for biocompatible semiconductor and gold nanocrystals with extended pH and ionic stability. *J. Mater. Chem.* **2008**, *18*, 4949.
(65) Huang, X.-Y.; Wang, H.-J.; Shi, J. Theoretical Study on Acidities of (S)-Proline Amide Derivatives in DMSO and Its Implications for Organocatalysis. *J. Phys. Chem. A* **2010**, *114*, 1068−1081.

https://dx.doi.org/10.1021/jacs.0c10592
J. Am. Chem. Soc. 2021, 143, 1873−1884

(66) Dunn, M. H.; Konstandaras, N.; Cole, M. L.; Harper, J. B. Targeted and Systematic Approach to the Study of pKa Values of Imidazolium Salts in Dimethyl Sulfoxide. *J. Org. Chem.* **2017**, *82*, 7324−7331.
(67) Zeng, B.; Palui, G.; Zhang, C.; Zhan, N.; Wang, W.; Ji, X.; Chen, B.; Mattoussi, H. Characterization of the Ligand Capping of Hydrophobic CdSe−ZnS Quantum Dots Using NMR Spectroscopy. *Chem. Mater.* **2018**, *30*, 225−238.
(68) Zhang, C.; Jin, Z.; Zeng, B.; Wang, W.; Palui, G.; Mattoussi, H. Characterizing the Brownian Diffusion of Nanocolloids and Molecular Solutions: Diffusion-Ordered NMR Spectroscopy vs Dynamic Light Scattering. *J. Phys. Chem. B* **2020**, *124*, 4631−4650.
(69) Carril, M.; Padro, D.; del Pino, P.; Carrillo-Carrion, C.; Gallego, M.; Parak, W. J. In situ detection of the protein corona in complex environments. *Nat. Commun.* **2017**, *8*, 1542.
(70) Padro, D.; Cienskowski, P.; Lopez-Fernandez, S.; Chakraborty, I.; Carrillo-Carrion, C.; Feliu, N.; Parak, W. J.; Carril, M. Toward Diffusion Measurements of Colloidal Nanoparticles in Biological Environments by Nuclear Magnetic Resonance. *Small* **2020**, *16*, 2001160.
(71) Stejskal, E. O.; Tanner, J. E. Spin Diffusion Measurements: Spin Echoes in the Presence of a Time-Dependent Field Gradient. *J. Chem. Phys.* **1965**, *42*, 288−292.
(72) Edward, J. T. Molecular volumes and the Stokes-Einstein equation. *J. Chem. Educ.* **1970**, *47*, 261.
(73) Wang, W.; van Niekerk, E. A.; Zhang, Y.; Du, L.; Ji, X.; Wang, S.; Baker, J. D.; Groeniger, K.; Raymo, F. M.; Mattoussi, H. Compact, "Clickable" Quantum Dots Photoligated with Multifunctional Zwitterionic Polymers for Immunofluorescence and In Vivo Imaging. *Bioconjugate Chem.* **2020**, *31*, 1497−1509.
(74) Arduengo, A. J.; Dixon, D. A.; Kumashiro, K. K.; Lee, C.; Power, W. P.; Zilm, K. W. Chemical Shielding Tensor of a Carbene. *J. Am. Chem. Soc.* **1994**, *116*, 6361−6367.
(75) Chianese, A. R.; Zeglis, B. M.; Crabtree, R. H. Unexpected oxidative C−C cleavage in the metallation of 2-substituted imidazolium salts to give N-heterocyclic carbene complexes. *Chem. Commun.* **2004**, 2176−2177.
(76) Marchione, D.; Izquierdo, M. A.; Bistoni, G.; Havenith, R. W. A.; Macchioni, A.; Zuccaccia, D.; Tarantelli, F.; Belpassi, L. 13C NMR Spectroscopy of N-Heterocyclic Carbenes Can Selectively Probe σ Donation in Gold(I) Complexes. *Chem. - Eur. J.* **2017**, *23*, 2722−2728.
(77) Thiel, K.; Zehbe, R.; Roeser, J.; Strauch, P.; Enthaler, S.; Thomas, A. A polymer analogous reaction for the formation of imidazolium and NHC based porous polymer networks. *Polym. Chem.* **2013**, *4*, 1848−1856.
(78) Rodríguez-Castillo, M.; Laurencin, D.; Tielens, F.; van der Lee, A.; Clément, S.; Guari, Y.; Richeter, S. Reactivity of gold nanoparticles towards N-heterocyclic carbenes. *Dalton Trans.* **2014**, *43*, 5978−5982.
(79) MacLeod, M. J.; Johnson, J. A. PEGylated N-Heterocyclic Carbene Anchors Designed To Stabilize Gold Nanoparticles in Biologically Relevant Media. *J. Am. Chem. Soc.* **2015**, *137*, 7974−7977.
(80) Wu, M.; Vartanian, A. M.; Chong, G.; Pandiakumar, A. K.; Hamers, R. J.; Hernandez, R.; Murphy, C. J. Solution NMR Analysis of Ligand Environment in Quaternary Ammonium-Terminated Self-Assembled Monolayers on Gold Nanoparticles: The Effect of Surface Curvature and Ligand Structure. *J. Am. Chem. Soc.* **2019**, *141*, 4316−4327.
(81) Westmoreland, D. E.; López-Arteaga, R.; Weiss, E. A. N-Heterocyclic Carbenes as Reversible Exciton-Delocalizing Ligands for Photoluminescent Quantum Dots. *J. Am. Chem. Soc.* **2020**, *142*, 2690−2696.
(82) Wang, W.; Kong, Y.; Jiang, J.; Tian, X.; Li, S.; Akshath, U. S.; Tiede, C.; Hondow, N.; Yu, A.; Guo, Y.; Zhou, D. Photon induced quantum yield regeneration of cap-exchanged CdSe/CdS quantum rods for ratiometric biosensing and cellular imaging. *Nanoscale* **2020**, *12*, 8647−8655.
(83) Manna, L.; Scher, E. C.; Li, L.-S.; Alivisatos, A. P. Epitaxial Growth and Photochemical Annealing of Graded CdS/ZnS Shells on Colloidal CdSe Nanorods. *J. Am. Chem. Soc.* **2002**, *124*, 7136−7145.
(84) Lakowicz, J. R. *Principles of Fluorescence Spectroscopy*, 3rd ed.; Springer US: 2006.
(85) Lynch, I.; Dawson, K. A. Protein-nanoparticle interactions. *Nano Today* **2008**, *3*, 40−47.
(86) Tsai, D.-H.; Davila-Morris, M.; DelRio, F. W.; Guha, S.; Zachariah, M. R.; Hackley, V. A. Quantitative Determination of Competitive Molecular Adsorption on Gold Nanoparticles Using Attenuated Total Reflectance−Fourier Transform Infrared Spectroscopy. *Langmuir* **2011**, *27*, 9302−9313.
(87) Perng, W.; Palui, G.; Wang, W.; Mattoussi, H. Elucidating the Role of Surface Coating in the Promotion or Prevention of Protein Corona around Quantum Dots. *Bioconjugate Chem.* **2019**, *30*, 2469−2480.
(88) Debayle, M.; Balloul, E.; Dembele, F.; Xu, X.; Hanafi, M.; Ribot, F.; Monzel, C.; Coppey, M.; Fragola, A.; Dahan, M.; Pons, T.; Lequeux, N. Zwitterionic polymer ligands: an ideal surface coating to totally suppress protein-nanoparticle corona formation? *Biomaterials* **2019**, *219*, 119357.
(89) Arabzadeh Nosratabad, N.; Jin, Z.; Du, L.; Thakur, M.; Mattoussi, H. N-Heterocyclic Carbene-Stabilized Gold Nanoparticles: Mono versus Multidentate Ligands. *Chem. Mater.*, DOI: 10.1021/acs.chemmater.0c03918, accepted.

https://dx.doi.org/10.1021/jacs.0c10592
J. Am. Chem. Soc. 2021, 143, 1873−1884